Research Article | Vol. 27, No. 6 | 18 Mar 2019 | OPTICS EXPRESS 8186
Optics EXPRESS

Intensity noise and bandwidth analysis of nanolasers via optical injection

ZIJUN CHEN,[1] SURUJ S. DEKA,[1] SI HUI PAN,[2] SIZHU JIANG,[1] CHENG-YI FANG,[3] YESHAIAHU FAINMAN,[1] AND ABDELKRIM EL AMILI[1,*]

[1]*Department of Electrical and Computer Engineering, University of California at San Diego, La Jolla, California 92093-0407, USA*
[2]*Department of Physics, University of California at San Diego, La Jolla, California 92093-0407, USA*
[3]*Department of Materials Science and Engineering, University of California at San Diego, La Jolla, California 92093-0407, USA*
[*]*aelamili@eng.ucsd.edu*

Abstract: A measurement method that can be used to extract the relative intensity noise of a nanolaser is introduced and analyzed. The method is based on optical injection of emission from a nanolaser serving as a master oscillator, transferring its intensity fluctuations to a low-noise semiconductor laser serving as a slave oscillator. Using the stochastic rate equation formalism, we demonstrate that the total relative intensity noise of the system is a weighted superposition of the relative intensity noise of individual lasers. We further discuss the analytical relations that can be used to extract the relative intensity noise spectrum of a nanolaser. Finally, we use mutual correlation as a mathematical tool to quantify the degree of resemblance between the injected and extracted intensity fluctuations, theoretically confirming that the spectra are at least 97% correlated within the 3-dB bandwidth when an injection strength is chosen properly.

1. Introduction

The development of coherent, nanoscale light sources is motivated by (i) the need in small footprint, fast response lasers with high energy efficiency to enable the realization of scalable chip-scale photonic integrated circuits (PIC) [1, 2] and (ii) creation of deeply subwavelength resonant cavity light emitters to enable the studies of cavity quantum electrodynamics [3, 4]. It is well known that in nanoscale light emitters/nanolasers, the fraction of spontaneous emission that is funneled into the lasing mode is enhanced. The figure-of-merit of this enhancement is called the spontaneous emission factor, β. The high-β in nanolasers results from significant reduction in the number of permissible cavity modes, consequently leading to lower lasing threshold. Additional studies [5–8] also show that the high-β light sources are suitable for high-speed direct modulation of such light emitters. However, in addition to high turn-on energy efficiency and fast modulation speed, telecommunication applications also require low noise performance to assure a high signal-to-noise ratio in detection processes at the receiver. Specifically, the signal-to-noise ratio of a coherent light source is inversely proportional to its relative intensity noise (RIN), which is defined by the autocorrelation of power fluctuations in an optical signal normalized by the square of its average power.

Although the onset lasing threshold of nanolasers have been investigated [9, 10], experimental studies of their relative intensity noise have not been reported yet. In fact, the RIN measurement in nanolasers remains a challenge because of their low power emission, which is on the order of pico- to micro-watts [8, 11]. In contrast, commercially available continuous-wave laser diodes at 1550 nm wavelength can typically provide output of 1-100 mW. The low emission power in nanolasers precludes the use of well-established RIN measurement techniques that are commonly used for characterization of conventional lasers. In this manuscript, we address this challenge

#357556 https://doi.org/10.1364/OE.27.008186
Journal © 2019 Received 14 Jan 2019; revised 15 Feb 2019; accepted 21 Feb 2019; published 6 Mar 2019

Optics EXPRESS

and demonstrate theoretically that an optical injection technique can be employed for indirect measurement of a nanolaser's RIN. Optical injection schemes have been commonly used to imprint high quality radiation properties of a low power master laser to control and improve spectral properties of a high-power slave laser with poor spectral properties [12]. In this approach, when a slave laser is injected with the emission from a low noise master laser, the spectral properties of the slave laser can be improved and consequently achieve a narrower linewidth emission. Here, in contrast, we use optical injection in an unconventional way to probe the nanolaser's RIN, by injecting emission from a "master" nanolaser into a low noise "slave" laser. In the following, we analyze the injection system and show that the measured RIN of the overall cascade system allows one to extract the RIN contribution of a nanolaser. We first analyze our system model using a set of stochastic rate equations and derive the RIN of the overall system in Sect. 2. Then in Sect. 3 we derive the transfer function of the "slave" laser using small signal analysis, followed by Sect. 4, where we derive the RIN spectrum of the injected laser and discuss two methods to extract the RIN of a nanolaser from the measured RIN of the cascaded system. Concluding remarks and discussions are provided in the last section.

2. Coupled laser rate equation

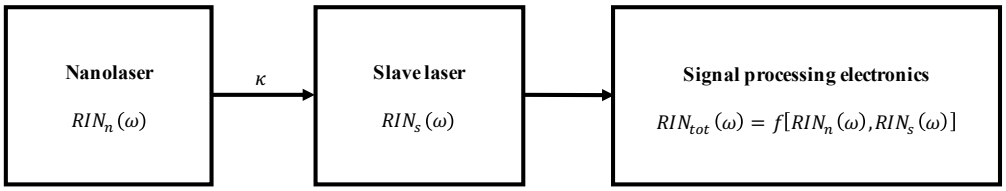

Fig. 1. The block diagram of an optical injection scheme. RIN: the intrinsic relative intensity noise; κ: the injection strength; $f[\cdot]$: an arbitrary function that is under investigation.

We adopt the rate equation formalism to model photon-carrier dynamics of a coupled system. Our objective is to study the photon-carrier interactions, and ultimately extract the RIN of a nanolaser, using the injection scheme depicted schematically in Fig. 1. The system consists of a "master" nanolaser that injects a fraction $\kappa^{1/2}$ of its emitted light field into a low noise semiconductor laser, which serves as a "slave" oscillator. The measured total RIN of the injection system includes the contributions of both "master" and "slave" oscillators.

The photon-carrier dynamics of the injection system are investigated using stochastic coupled rate equations. The dynamical behavior of the "slave" laser is given by [5, 13, 14]:

$$\frac{dS_s(t)}{dt} = \Gamma_s S_s(t)\left\{g_{0,s}\left[N_s(t) - N_{0,s}\right] - \frac{1}{\tau_{p,s}}\right\} + \frac{\Gamma_s F_s \beta_s N_s(t)}{\tau_{r,s}} + \frac{\kappa S_n(t)}{\tau_{rt,s}} + L_{S,s}(t), \tag{1}$$

$$\frac{dN_s(t)}{dt} = P_s - g_{0,s}\left[N_s(t) - N_{0,s}\right] S_s(t) - \left[\frac{F_s\beta_s - (1-\beta_s)}{\tau_{r,s}} + \frac{1}{\tau_{nr,s}}\right] N_s(t) + L_{N,s}(t), \tag{2}$$

where S is the photon density, N is the carrier density, P is the continuous-wave pump rate, L is the Langevin noise source, κ is the injection strength, and τ is the relaxation lifetime. The physical meanings of these laser parameters are detailed in Table 1. Additionally, the subscripts n and s are used to denote the nanolaser and the "slave" laser, respectively. The rate equations for the "master" nanolaser can be retrieved from Eqs. (1) and (2) by setting κ to zero and replacing the subscript s by n.

Since classical electromagnetism is inadequate in describing stochastic processes such as the rate equations in Eqs. (1) and (2), the Langevin method is used in our analysis. The Langevin noise sources are assumed to be memoryless random processes. Though this means that the

Optics EXPRESS

Table 1. Laser parameters

	Symbols	Nanolaser	Slave laser [15]	Unit
Modal confinement factor	Γ	0.6	0.4	-
Photon lifetime	τ_p	2.88	3	ps
Radiative carrier lifetime	τ_r	1	1	ns
Non-radiative carrier lifetime	τ_{nr}	1	1	ns
Round-trip time	τ_{rt}	-	8.63	ps
Differential gain coefficient	g_0	4.29×10^{-6}	2.14×10^{-6}	cm^3/s
Lasing wavelength	λ	1550	1550	nm
Carrier density at transparency	N_0	2×10^{18}	1×10^{18}	cm^{-3}
Modal volume	V_p	9.82×10^{-14}	3.75×10^{-10}	cm^3
Volume of the active region	V	5.89×10^{-14}	1.5×10^{-10}	cm^3
Spontaneous emission factor	β	0.2	3×10^{-5}	-
Purcell factor [8]	F	67.22	1	-

Langevin noise sources average to zero over a finite time interval, their characteristics can still be quantified through mutual correlation [13, 14],

$$\left\langle L_i(t) L_j^*(t-\tau) \right\rangle = W_{ij}\delta(\tau). \tag{3}$$

Here, the angle brackets denote ensemble averaging and W_{ij} is the correlation strength between Langevin noise sources. As we will demonstrate below, the Langevin noise sources are needed to calculate the laser RINs. In addition, the Langevin noise sources of the two laser oscillators are assumed to be uncorrelated.

3. Small signal analysis

The coupled rate equations are linearized by assuming a negligible gain compression coefficient. The linearization is performed such that the rate equations are self-consistent with a first-order perturbative calculation. Also because of linearization, the presented method is inapplicable in pulsed-pumped lasers. We further assume that there is no detuning in the lasing wavelengths and require the injection path length to be greater than the coherence length of the nanolaser. As a reference, the coherence time of the chosen nanolaser is typically on the order of 1 ns [16]. This corresponds to an injection path length of 30 cm in air (20 cm in an optical fiber). If this condition is satisfied, the formalism is simplified by eliminating interference-induced instability [12, 17]. The analysis is thus focused solely on the discussion of intensity noise.

Linear system analysis is used to approximate the fluctuations in particle densities, as small signal responses [13, 14]. In the absence of pump fluctuations, the "slave's" photon and carrier noise spectra are given by

$$\begin{bmatrix} \delta\tilde{N}_s(\omega) \\ \delta\tilde{S}_s(\omega) \end{bmatrix} = \frac{1}{D_s(\omega)} \begin{bmatrix} i\omega + \gamma_{SS,s} & -\gamma_{NS,s} \\ \gamma_{SN,s} & i\omega + \gamma_{NN,s} \end{bmatrix} \cdot \begin{bmatrix} \tilde{L}_{N,s}(\omega) \\ \tilde{L}_{S,s}(\omega) + \dfrac{\kappa}{\tau_{rt,s}}\delta\tilde{S}_n(\omega) \end{bmatrix}, \tag{4}$$

Optics EXPRESS

where

$$D_s(\omega) = \left(\omega_{0,s}^2 - \omega^2\right) + i\omega\xi_s. \tag{5}$$

Here, ω is the Fourier angular frequency, ω_0 is the natural angular frequency, ξ is the damping coefficient, and γ are the small signal parameters (see Appendix A). The small signal $\delta\tilde{S}_n$ injected by the nanolaser is obtained from Eqs. (4) and (5) by setting κ to zero and replacing the subscript s by n. The contributions by nonradiative processes to the steady state responses are neglected in Eq. (4). This approximation is made after the contributions by nonradiative processes are accounted for in both the steady state and small signal analysis. The contributions of nonradiative processes are retained, however, in the noise analysis such that the intensity noise level is appropriately evaluated. In other words, the nonradiative carrier lifetime for both lasers are retained in the small signal analysis to account for their contributions to noise, but neglected in the steady state responses due to their negligible contributions to the light-in-light-out curve.

The photon density fluctuation of the "slave" laser, $\delta\tilde{S}_s$, consists of contributions from both the photon noise source $\tilde{L}_{S,s}$ and the photon density fluctuation of the nanolaser, $\delta\tilde{S}_n$, which is filtered by the "slave's" resonant cavity. Note that the weight which precedes the term $\delta\tilde{S}_n$ in Eq. (4) is a transfer function. To demonstrate this fact, consider the case in which all Langevin noise sources are absent, which allows us to arrive at the transfer function of the "slave" laser:

$$H_s(\omega) \equiv \frac{\delta\tilde{S}_s}{\delta\tilde{S}_n} = \frac{\kappa}{\tau_{rt,s}} \frac{i\omega + \gamma_{NN,s}}{D_s(\omega)}. \tag{6}$$

The form of Eq. (6) can be recognized as a second-order low-pass filter. The prior knowledge of the transfer function is essential to extract the properties associated with the photon density fluctuation in the nanolaser. Moreover, the relaxation oscillation angular frequency $\omega_{R,s}$ is given by

$$\omega_{R,s} = \omega_{0,s}\sqrt{1 - \frac{\xi_s^2}{2\omega_{0,s}^2}}. \tag{7}$$

We observe from Eq. (7) that when either the natural angular frequency or the damping coefficient are modified under external injection, there will be a change in the slave's relaxation oscillation angular frequency. In the absence of damping rate, the relaxation oscillation frequency is equal to $\omega_{0,s}$ and hence the name "natural" angular frequency.

4. Relative intensity noise

Next we use small signal response to derive the total RIN of the injection system from which the intrinsic RIN of a nanolaser can be extracted. The definition of a single-sided RIN spectra is first derived using the Wiener-Khinchin theorem [14]:

$$RIN(\omega) \equiv \frac{PSD(\omega)}{\bar{S}^2} = \frac{\left\langle \delta\tilde{S}(\omega)\delta\tilde{S}^*(\omega)\right\rangle}{\bar{S}^2}. \tag{8}$$

The overbar denotes the steady state response. Note that the noise power spectral density is given by the variance of the small signal response. Using Eqs. (4) and (8) the total RIN is then determined as

$$RIN_{tot}(\omega) = H_f(\omega)\, RIN_n(\omega) + RIN_s(\omega) \tag{9}$$

where

$$H_f(\omega) = \frac{\bar{S}_n^2}{\bar{S}_s^2} |H_s(\omega)|^2. \tag{10}$$

Here, H_f is the filtering function, RIN_n is the intrinsic RIN of the isolated nanolaser, and RIN_s is the intrinsic relative intensity noise of the "slave" laser. The explicit form of the intrinsic RINs

Optics EXPRESS

are presented in Appendix B. It is clear from Eq. (9) that the RIN of the injected laser is additive. We verify that if the external injection is absent, the "slave's" intrinsic RIN returns to the case in which the "slave" laser is in complete isolation.

4.1. Low-noise method

We next demonstrate a method to extract the RIN of the nanolaser by considering its contribution in the total RIN. First, we assume that the laser RIN of the "master" nanolaser dominates among other additive noises that can appear in practice. It would therefore be ideal to use a low-noise "slave" laser, such that a consistent approximation can be made to further simplify Eq. (9) yielding,

$$RIN_{tot}(\omega) \approx H_f(\omega)\, RIN_n(\omega). \tag{11}$$

By measuring the average photon densities and the "slave's" laser parameters, the filtering function can be determined from Eqs. (6) and (10). The contribution of the nanolaser, RIN_n, can then be extracted using Eq. (11) with simple algebraic manipulation. However, this technique does presume that the filtering function can be extracted experimentally. Since the optical power level is high enough in conventional semiconductor low-noise lasers, the transfer function can be, therefore, measured experimentally using conventional methods [18].

4.2. Direct estimation method

An alternative method in which RIN_n is estimated directly from RIN_{tot} can be also used. To show this effect, Eq. (9) is solved numerically at two selected injection strengths and plotted in Fig. 2. Comparing the results in Fig. 2(a) and 2(b) we observe two notable changes in RIN_{tot} spectrum as the injection strength is changed: (1) a shifted relaxation oscillation frequency and (2) an increased noise level at the flat band. When the injection strength κ is changed from 1% to 25%, the total RIN increases by modifying the intrinsic RIN of the "slave" laser. This observation supports the fact that the direct estimation method can be used to extract the injected RIN directly from the total RIN, given that the injection strength κ is appropriately chosen. The disadvantage incurred in this process is that the additional poles due to the cascaded laser cavities are retained in the total system RIN. Such approach limits the degree to which the nanolaser's RIN can be directly estimated with the total RIN consisting of a -40 dB/Hz per decade roll-off

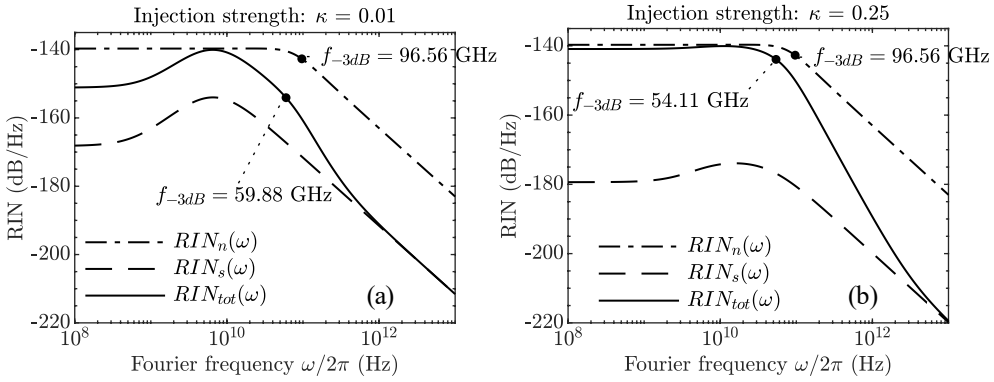

Fig. 2. Total RIN at two selected injection strength (a) κ = 0.01 and (b) κ = 0.25. The master and the slave are pumped at thrice and twice of their respective threshold levels. In determining the threshold of the nanolaser, the carrier density is first calculated as a function of pump rate. The threshold is then determined graphically by extrapolating two regions around the kink in the carrier density. This prediction can be translated into an experimental measurement through its corresponding light-in-light-out curve.

Optics EXPRESS

after its 3-dB frequency. Moreover, an enhancement of the resonant peak is also observed. The shift in resonance can be explained by Eq. (6) with the natural angular frequency of the "slave" laser written explicitly as:

$$\omega_{0,s}^2 \approx \frac{g_{0,s}\bar{S}_s}{\tau_{p,s}} + \frac{1}{\tau_{p,s}\tau_{r,s}} + \frac{\Gamma_s g_{0,s}\left(\bar{N}_s - N_{0,s}\right)}{\tau_{r,s}}, \tag{12}$$

where

$$\bar{S}_s = \frac{1}{1/\tau_{p,s} - \Gamma_s g_{0,s}(\bar{N}_s - N_{0,s})} \cdot \frac{\kappa \bar{S}_n}{\tau_{rt,s}} \tag{13}$$

The spontaneous emission factor of the "slave" laser was neglected in the process of arriving at Eqs. (12) and (13). It is evident from Eqs. (12) and (13) that the shifted relaxation oscillation frequency depends on the injection strength κ. When the relaxation oscillation frequency increases, the increased roll-off inevitably prevents a direct estimation of the nanolaser's modulation bandwidth.

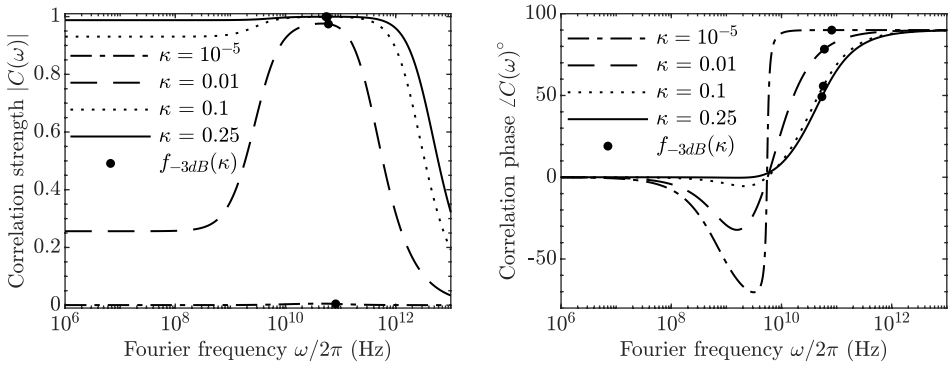

Fig. 3. (a) Correlation strength and (b) phase of the complex mutual correlation function. The 3-dB points correspond to the 3-dB bandwidth of the total RIN spectra. The pump levels are identical to that of Fig. 2.

To better quantify how the intensity fluctuations of the "master" nanolaser influence the intensity fluctuations of the "slave" laser, we use a complex mutual correlation function defined by

$$C(\omega) = \frac{\left\langle \delta\tilde{S}_s(\omega)\delta\tilde{S}_n^*(\omega)\right\rangle}{\sqrt{\left\langle \delta\tilde{S}_s(\omega)\delta\tilde{S}_s^*(\omega)\right\rangle \left\langle \delta\tilde{S}_n(\omega)\delta\tilde{S}_n^*(\omega)\right\rangle}} \tag{14}$$

Numerical evaluations of Eq. (14) are shown in Fig. 3. We observe that the correlation spectra improved in both the bandwidth and magnitude as the injection strength increases. When the injection strength is at 25%, the injected and extracted signals are at least 97% correlated within the 3-dB bandwidth of RIN_{tot}, demonstrating quantitatively a band-limited RIN extraction. Although the correlation strength in principle approaches unity as the injection strength increases, it is somewhat impractical. For instance, 99.7% correlation strength is achieved within the 3-dB bandwidth of the total RIN when κ is at 50%. Additionally, the photon density fluctuations are highly correlated within the region in which the phase valley diminishes, suggesting that this is a sufficient condition to determine the injection strength to achieve an optimal resemblance of the injected signal. From Eq. (14), the absence of zero-crossing in the correlation phase requires

$$\xi_s \gamma_{NN,s} > \omega_{0,s}^2. \tag{15}$$

Optics EXPRESS

This condition can be used to calculate the desired injection strength in an experimental measurement.

The optimal condition Eq. (15) aims to achieve near unity correlation strength within the 3-dB bandwidth. In practice, if a band-limited correlation strength less than near unity is tolerable, the criterion can be written as

$$\xi_s \gamma_{NN,s} = \left(\frac{\omega_{0,s}}{m}\right)^2 \tag{16}$$

where m is the degree of freedom that regulates the trade-off between a minimum power injection and a tolerable correlation strength. The numerical solution of Eq. (16) is shown in Fig. 4. Firstly, Fig. 4(a) demonstrates a trade-off between minimally required power at chosen values of m. In our case, a 97% correlation strength corresponds to $m \approx 1.6$. The value of m is jointly determined by the chosen injection strength and pump power. If the "master" nanolaser consists of an averaged output power that is greater than the minimally required power, which is shown as the blue curve in Fig. 4(b), the correlation strength in this case is bounded between 97% and 100%. An improvement in the correlation strength can be further made as m approaches to 1, which is suggested by Eq. (15). We note that the correlation strength can be improved at most an additional 3% and the difference in the required power differs by one order of magnitude. The observed difference in the required power emission is consistent with results shown in Fig. 3(a).

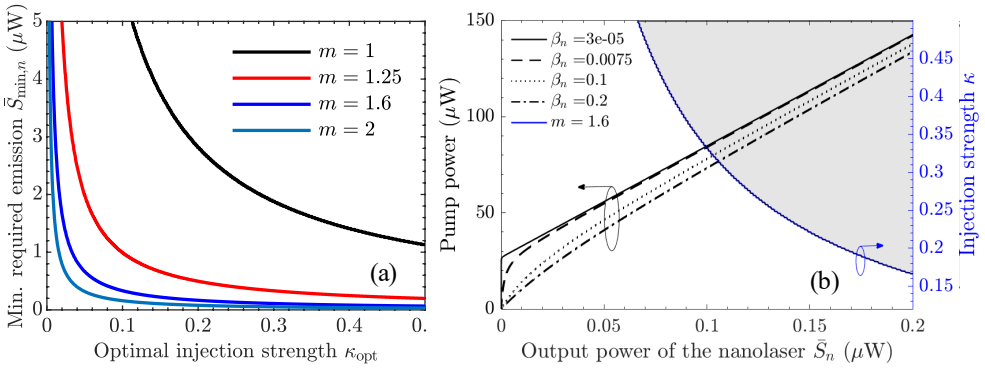

Fig. 4. (a) Minimally required power emitted by the nanolaser at selected values of m (b) parameters that yield a high correlation strength ($\geq$ 97%) within the 3-dB bandwidth appear in the gray region. The pump rate and photon density are converted to power as suggested in [14].

5. Conclusion

In summary, we introduce and theoretically investigate the validity of extracting the RIN of a nanolaser using the optical injection scheme. Stochastic rate equations have been used to derive the RIN of the injected overall laser system. We demonstrate that the total RIN is a weighted sum of the intrinsic RIN of the two laser oscillators. This simple additive relation enables us to extract the RIN of a nanolaser. We then discussed two possible recovery methods: the low-noise method and the direct estimation method. We arrived at the former when a low noise "slave" laser is employed. In principle, the "slave's" intrinsic RIN is negligible, thus allowing one to extract the nanolaser's RIN through simple algebraic manipulation. The advantage of this method is that the extracted RIN consists of information about the nanolaser's intrinsic noise level and its modulation bandwidth. This low-noise method, however, requires precise knowledge of the "slave's" laser parameters. Specifically, the transfer function of the "slave" laser must be precisely known. In contrast, although the second, direct estimation method, offers a way to circumvent

Optics EXPRESS

the issue of lack of information about the "slave" laser, it suffers in bandwidth extraction due to the cascaded cavities. We demonstrated that with our assumptions, the injected and extracted spectra are at least 97% correlated within the 3-dB bandwidth of the total RIN at an injection strength of 25%. Consequently, we derived a sufficient condition that allows us to determine the optimal injection strength and conclude that the second, direct estimation method, is accurate only within the 3-dB bandwidth of the measured RIN spectrum. We furthermore considered a less restrictive condition and demonstrated the trade-off between minimally required injection power and correlation strength. In doing so the proposed scheme is more flexible to implement in practice.

Appendix A: Small signal parameters

The small signal parameters are

$$\gamma_{NN,\ell} = g_{0,\ell}\bar{S}_\ell + \frac{\beta_\ell F_\ell + (1-\beta_\ell)}{\tau_{r,\ell}}, \tag{17}$$

$$\gamma_{SS,\ell} = \frac{1}{\tau_{p,\ell}} - \Gamma_\ell g_{0,\ell}\left(\bar{N}_\ell - N_{0,\ell}\right), \tag{18}$$

$$\gamma_{NS,\ell} = g_{0,\ell}\left(\bar{N}_\ell - N_{0,\ell}\right), \tag{19}$$

$$\gamma_{SN,\ell} = \Gamma_\ell g_{0,\ell}\bar{S} + \frac{\Gamma_\ell F_\ell \beta_\ell}{\tau_{r,\ell}}, \tag{20}$$

$$\omega_{0,\ell}^2 = \gamma_{NN,\ell}\gamma_{SS,\ell} + \gamma_{NS,\ell}\gamma_{SN,\ell}, \tag{21}$$

$$\xi_\ell = \gamma_{NN,\ell} + \gamma_{SS,\ell}. \tag{22}$$

The derived expressions are valid for both the nanolaser ($\ell = n$) and the slave laser ($\ell = s$). Despite the form of the small signal parameters are identical, the laser parameters and average particle densities are numerically different.

Appendix B: Correlation strength of Langevin noise sources

Using the definition of the single-sided RIN spectra, we have arrived at

$$RIN_\ell(\omega) = \frac{\gamma_{SN,\ell}^2\left\langle \tilde{L}_{N,\ell}\tilde{L}_{N,\ell}^*\right\rangle}{|D(\omega)|^2\,\bar{S}_\ell^2} + \frac{\left(\gamma_{NN,\ell}^2+\omega^2\right)\left\langle \tilde{L}_{S,\ell}\tilde{L}_{S,\ell}^*\right\rangle}{|D(\omega)|^2\,\bar{S}_\ell^2} + \frac{2\gamma_{SN,\ell}\gamma_{NN,\ell}\left\langle \tilde{L}_{S,\ell}\tilde{L}_{N,\ell}^*\right\rangle}{|D(\omega)|^2\,\bar{S}_\ell^2}, \tag{23}$$

where the correlation strength between the Langevin noise sources of the slave laser are given by

$$\left\langle \tilde{L}_{S,s}\tilde{L}_{N,s}^*\right\rangle = \left\langle \tilde{L}_{N,s}\tilde{L}_{S,s}^*\right\rangle = -\frac{\Gamma_s}{V_s}\left[g_{0,s}\left(\bar{N}_s - N_{0,s}\right)\bar{S}_s + \frac{F_s\beta_s\bar{N}_s}{\tau_{r,s}}\right], \tag{24}$$

$$\left\langle \tilde{L}_{N,s}\tilde{L}_{N,s}^*\right\rangle = \frac{\bar{P}_s}{V_s} + \left[\frac{F_s\beta_s + (1-\beta_s)}{\tau_{r,s}} + \frac{1}{\tau_{nr,s}}\right]\frac{\bar{N}_s}{V_s} + \frac{g_{0,s}}{V_s}(\bar{N}_s + N_{0,s})\bar{S}_s, \tag{25}$$

$$\left\langle \tilde{L}_{S,s}\tilde{L}_{S,s}^*\right\rangle = \frac{\bar{S}_s}{\tau_{p,s}V_s} - \frac{V_s}{V_{p,s}}\left\langle \tilde{L}_{S,s}\tilde{L}_{N,s}^*\right\rangle + \frac{\kappa\bar{S}_n}{\tau_{rt,s}V_{p,s}}. \tag{26}$$

The correlation strength among the noise sources are derived by counting the average number of particles that are exchanged between the photon and carrier reservoirs [13, 14]. The expressions for both the RIN and correlation strength of a nanolaser are obtained by setting κ to zero and replacing the subscript s (or ℓ) by n.

Optics EXPRESS

Funding

Defense Advanced Research Projects Agency (DARPA) and DARPA NLM; Office of Naval Research (ONR) Multidisciplinary University Research Initiative (MURI); National Science Foundation (NSF) (DMR-1707641, CBET-1704085, ECCS-1405234, ECCS-1644647, CCF-1640227, ECCS-1507146); NSF ERC CIAN; Semiconductor Research Corporation (SRC); Army Research Office (ARO); Cymer Corporation.

References

1. M. J. Heck and J. E. Bowers, "Energy efficient and energy proportional optical interconnects for multi-core processors: Driving the need for on-chip sources," IEEE J. Sel. Top. Quantum Electron. **20**, 332–343 (2014).
2. Z. Zhou, B. Yin, and J. Michel, "On-chip light sources for silicon photonics," Light. Sci. & Appl. **4**, e358 (2015).
3. H. Walther, "Experiments on cavity quantum electrodynamics," Phys. Reports **219**, 263–281 (1992).
4. Q. Gu, B. Slutsky, F. Vallini, J. S. Smalley, M. P. Nezhad, N. C. Frateschi, and Y. Fainman, "Purcell effect in sub-wavelength semiconductor lasers," Opt. Express **21**, 15603–15617 (2013).
5. E. K. Lau, A. Lakhani, R. S. Tucker, and M. C. Wu, "Enhanced modulation bandwidth of nanocavity light emitting devices," Opt. Express **17**, 7790–7799 (2009).
6. T. Suhr, N. Gregersen, K. Yvind, and J. Mørk, "Modulation response of nanoleds and nanolasers exploiting purcell enhanced spontaneous emission," Opt. Express **18**, 11230–11241 (2010).
7. S. Matsuo, A. Shinya, T. Kakitsuka, K. Nozaki, T. Segawa, T. Sato, Y. Kawaguchi, and M. Notomi, "High-speed ultracompact buried heterostructure photonic-crystal laser with 13 fj of energy consumed per bit transmitted," Nat. Photonics **4**, 648–654 (2010).
8. C.-Y. A. Ni and S. L. Chuang, "Theory of high-speed nanolasers and nanoleds," Opt. Express **20**, 16450–16470 (2012).
9. R. Hostein, R. Braive, L. Le Gratiet, A. Talneau, G. Beaudoin, I. Robert-Philip, I. Sagnes, and A. Beveratos, "Demonstration of coherent emission from high-β photonic crystal nanolasers at room temperature," Opt. Lett. **35**, 1154–1156 (2010).
10. W. W. Chow, F. Jahnke, and C. Gies, "Emission properties of nanolasers during the transition to lasing," Light. Sci. & Appl. **3**, e201 (2014).
11. M. Khajavikhan, A. Simic, M. Katz, J. Lee, B. Slutsky, A. Mizrahi, V. Lomakin, and Y. Fainman, "Thresholdless nanoscale coaxial lasers," Nature **482**, 204–207 (2012).
12. E. K. Lau, L. J. Wong, and M. C. Wu, "Enhanced modulation characteristics of optical injection-locked lasers: A tutorial," IEEE J. Sel. Top. Quantum Electron. **15**, 618–633 (2009).
13. G. Ghione, *Semiconductor devices for high-speed optoelectronics* (Cambridge University, 2009).
14. L. A. Coldren, S. W. Corzine, and M. L. Mashanovitch, *Diode lasers and photonic integrated circuits* (John Wiley & Sons, 2012).
15. A. Mahmoud, S. W. Mahmoud, and K. Abdelhady, "Modeling and simulation of dynamics and noise of semiconductor lasers under ntsc modulation for use in the catv technology," Beni-Suef Univ. J. Basic Appl. Sci. **4**, 99–108 (2015).
16. S. H. Pan, Q. Gu, A. El Amili, F. Vallini, and Y. Fainman, "Dynamic hysteresis in a coherent high-β nanolaser," Optica **3**, 1260–1265 (2016).
17. J. Ohtsubo, *Semiconductor lasers: stability, instability and chaos* (Springer, 2012).
18. G. Baili, M. Alouini, T. Malherbe, D. Dolfi, I. Sagnes, and F. Bretenaker, "Direct observation of the class-b to class-a transition in the dynamical behavior of a semiconductor laser," EPL **87**, 44005 (2009).